Prediction of low speed manoeuvring based on captive model tests: opportunities and limitations.

Katrien ELOOT[1], Marc VANTORRE[1,2]

katrien.eloot@lin.vlaanderen.be. marc.vantorre@lin.vlaanderen.be

[1] c/o Flanders Hydraulics Research, Berchemlei 115, B 2140 Antwerpen (Belgium)
[2] Ghent University (Department of Mechanical Construction and Production, Section Maritime Technology), Technologiepark Zwijnaarde 9, B 9052 Gent (Belgium)

Abstract: The Flemish waterways authorities are permanently concerned about safety of navigation to the Belgian harbours in order to maintain their present position in the European shipping market. Special attention is paid to the effect of the constant growth of ship dimensions, especially in the container traffic, to safe shipping traffic. Harbour manoeuvres are characterised by a great diversity and particularly low speed manoeuvring is brought more and more to the attention of the institutes involved in the prediction of ship manoeuvrability. Hydrodynamic forces induced at low speed and low or even reversed telegraph positions must be determined carefully both in deep and in shallow water. Some insight into the opportunities and limitations of mathematical modelling based on captive model tests could be obtained based on a thorough investigation started at Flanders Hydraulics Research. This paper will focus on results of model tests with a fourth generation containership with a draught of 15.0 m at an under keel clearance of 20%.

1. INTRODUCTION

At the MARSIM conference in 2003 (Kanazawa, Japan) two papers have been presented dealing with the issue of characterising the ship manoeuvring performance at (s)low speed [1], [2]. The need of formulating criteria which do not only rely to deep water and service speed such as the IMO Manoeuvrability Criteria do, has been recognised.

The prediction of low speed manoeuvring depends especially on the predictive power of simulation models and according to [1] the low speed confined water handling qualities of a new design could be determined by computer.

In [2] the formal mathematical model of Goodman and Roseman which takes into account all possible manoeuvres characterised by varying propeller loading, positive or negative ship velocity and positive or negative propeller rate, is considered to be the only simulation model which reproduces (with relatively good success) the slow speed manoeuvres in both deep and shallow water. This model is based on the ratio of propeller loading, expressed by η (the ship propulsion ratio) function of the apparent advance coefficient J':

$$\eta = \frac{\left(\eta_U\right)}{\eta} = \frac{J'_c}{J} \tag{1}$$

with J'_c the apparent advance coefficient at self propulsion. This propulsion ratio reaches specific values at the following situations:

- At self propulsion: $\eta = 1$
- At bollard pull: $\eta = \infty$
- At stopped propeller: $\eta = 0$

At Flanders Hydraulics Research a captive model test program with a fourth generation containership is completed, combining all possible combinations of ship velocities and propeller telegraph positions which occur during harbour manoeuvres. This comprehensive test program conducted in shallow water conditions could be a valuable tool for:

- the evaluation of hull, propeller and rudder forces to be incorporated in a manoeuvring simulation model
- the evaluation of the applicability of existing mathematical models and their convenience to predict harbour manoeuvres.

Some examples of these two subjects will be discussed in this paper.

2. MATHEMATICAL MODEL: GENERAL STRUCTURE

2.1. Introduction

A four quadrant operation model of the propeller is based on equation (10) and the following assumptions differ from the definition given by Harvald [3] (quadrants 2 en 4 have been swapped):

QUADRANT 2 $u > 0, n < 0$	**QUADRANT 1** $u > 0, n > 0$
QUADRANT 3 $u < 0, n < 0$	**QUADRANT 4** $u < 0, n > 0$
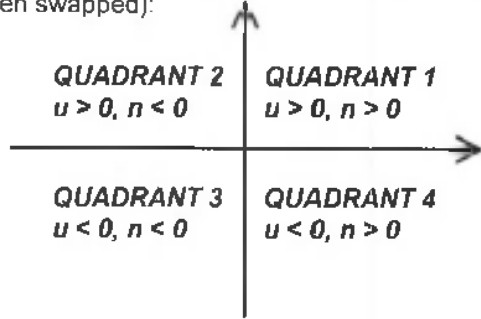
The quadrants correspond to the following operations:

☐ quadrant 1: running ahead
☐ quadrant 2: stopping from headway
☐ quadrant 3: running astern
☐ quadrant 4: stopping from sternway

Open water characteristics of the propeller and the rudder will be used for modelling.

2.2. General structure

The equations of motion in the horizontal plane are:

$$m\left(\dot{u} - vr - x_G r^2\right) = X_H + X_P + X_R$$
$$m\left(\dot{v} + ur + x_G \dot{r}\right) = Y_H + Y_P + Y_R \qquad (2)$$
$$I_{zz}\dot{r} + mx_G\left(\dot{v} + ur\right) = N_H + N_P + N_R$$

with $_H$ hull, $_P$ propeller and $_R$ rudder. Each force component at the right hand side of the equations (2) can be expressed as a combination of forces acting on the module itself and interaction terms.

2.3. Hull forces and moment

Hull force components have been discussed in [4] and are mainly caused by accelerations and velocities.

$$X_H = X_{\dot{u}}\dot{u} + X^{(\beta)}(u,v,0) + X^{(\gamma)}(u,0,r)$$
$$+ X^{(\beta,\gamma)}(0,v,r)$$
$$Y_H = Y_{\dot{v}}\dot{v} + Y_{\dot{r}}\dot{r} + Y^{(\beta)}(u,v,0) + Y^{(\gamma)}(u,0,r)$$
$$+ Y^{(\beta,\gamma)}(0,v,r) \qquad (3)$$

$$N_H = N_{\dot{r}}\dot{r} + N_{\dot{v}}\dot{v} + N^{(\beta)}(u,v,0) + N^{(\gamma)}(u,0,r)$$
$$+ N^{(\beta,\gamma)}(0,v,r)$$

The velocity dependent forces in (3) are expressed as tabular models, the following angles varying between [-180°, 180°]:

$$\beta = \text{Arc} \tan\left(\frac{-v}{u}\right) \qquad (4)$$

$$\gamma = \text{Arc}\tan\left(\frac{r l}{u}\right) = \text{Arc}\tan\left(\frac{r L_{pp}}{2u}\right) \qquad (5)$$

$$\text{Arc}\tan\left(\frac{r l}{v}\right) \qquad (6)$$

The expressions $f^{(\beta)}(u,v,0)$, $f^{(\gamma)}(u,0,r)$ and $f^{(\beta,\gamma)}(0,v,r)$ with f=X, Y or N are respectively the forces measured during pure sway (r = 0), pure yaw (v = 0) or the additional forces measured during a combination of sway and yaw.

2.4. Propeller induced forces and moment

The longitudinal force X_P is the most important component induced by the propeller. The model is based on the propeller open water characteristic $K_T(\varepsilon)$:

$$X_P = \left[1 - t_P\left(\varepsilon^*, \beta_P\right)\right]T_P \qquad (7)$$

with
$$T_P = \rho n^2 D_P^4 K_T(\varepsilon) \qquad (8)$$

The expressions for the propeller thrust T_P and the thrust deduction t_P are based on the MMG-model but some modifications are made and a four quadrant model of the propeller influence is introduced based on the advance angle ε, the apparent advance angle ε^*, the total inflow velocity U_P and the inflow angle β_P at the propeller during swaying and yawing.

$$\varepsilon = \text{Arctan}\left(\frac{\left(1 - w_P\left(\varepsilon^*, \beta_P\right)\right)U_P}{0.7\pi n D_P}\right) \qquad (9)$$

$$\varepsilon^* = \text{Arctan}\left(\frac{U_P}{0.7\pi n D_P}\right) \qquad (10)$$

$$U_P = \sqrt{u^2 + \left[v + x_P r\right]^2} \qquad (11)$$

$$\beta_P = \text{Arc}\tan\left(\frac{-\left(v + x_P r\right)}{u}\right) \qquad (12)$$

2.5. Rudder induced forces and moment

Based on the MMG-model the expressions for rudder forces and moment are:

$$X_R = (1 - t_R)F_X$$
$$Y_R = (1 + a_H)F_Y \qquad (13)$$
$$N_R = (x_R + a_H x_H)F_Y$$

t_R, a_H and x_H are interaction coefficients. The forces F_X and F_Y acting on the rudder itself can be modelled based on the open water characteristics of the rudder C_{FT} and C_{FN}:

$$F_X = \frac{\rho}{2} A_R V_R^2 \{C_{FT}(\alpha_R)\cos\delta_R - C_{FN}(\alpha_R)\sin\delta_R\}$$

$$F_Y = \frac{\rho}{2} A_R V_R^2 \{C_{FT}(\alpha_R)\sin\delta_R + C_{FN}(\alpha_R)\cos\delta_R\}$$

$$(14)$$

The entrance velocity V_R and the direction α_R of the flow into the rudder can be written as:

$$V_R = \sqrt{u_R^2 + v_R^2} \qquad (15)$$
$$\alpha_R = \delta_R + \delta_0 + \beta_R \qquad (16)$$

with δ_0 the zero rudder offset, δ_R the rudder angle and β_R the inflow angle into the rudder:

$$\beta_R = \text{Arctan}\left(\frac{-v_R}{u_R}\right) \qquad (17)$$

The inflow components into the rudder, u_R and v_R, are based on the MMG-model and can be written as:

$$u_R = u(1-w_R)\sqrt{\eta_R\left\{1+k\left(\sqrt{1+\frac{8K_T}{\pi J^2}}-1\right)\right\}^2 + (1-\eta_R)}$$

or

$$u_R = \zeta\left\{\eta_R\left[u_P + k\left(\sqrt{u_P^2 + \frac{8K_T n^2 D_P^2}{\pi}} - u_P\right)\right]^2 + (1-\eta_R)u_P^2\right\}^{\frac{1}{2}}$$

$$(18)$$

$$\zeta = \frac{1-w_R}{1-w_P} \qquad (19)$$

$$v_R = \delta_0 u_R + k_{HPR}(v + x_R r) \qquad (20)$$

where ζ denotes the ratio of the wake fraction at the rudder to the wake fraction at the propeller, k_{HPR} is the flow-straightening coefficient (hull-propeller-rudder combination) and η_R is the ratio of the propeller diameter to the rudder height.

3. PROGRAM OF CAPTIVE MODEL TESTS

An extensive program of captive model tests has been executed with a fully automated PMM-carriage at the *Towing Tank for Manoeuvres in Shallow Water (co-operation Flanders Hydraulics Research – Ghent University)*, Antwerp (Belgium). The main characteristics of the towing tank are 88 x 7 x 0.5 m³, with a useful length of 68 m.

Hull, propeller and rudder characteristics are summarised in table 1.

Table 1 Geometrical characteristics

Container carrier D		
Hull	Model scale	Full scale
L_{OA}	4.020 m	301.5 m
L_{PP}	3.864 m	289.8 m
B	0.537 m	40.3 m
d	0.200 m	15.0 m
C_B	0.61	
Propeller		
Z	5	5
D_P	0.1086 m	8.145 m
P/D_P	0.9696	0.9696
A_E/A_0	0.8	0.8
Rudder		
A_R	108 cm²	61 m²
Scale	1:75	

The test results concern a shallow water condition with an under keel clearance of 20% of the ship's draught; only in figure 1 results with 7% under keel clearance are displayed as well.

The test program consisted of following test types:

Stationary captive manoeuvring tests:
❑ straight-line tests with positive and negative forward speed;
❑ oblique towing tests with positive and negative forward speed.

Non-stationary captive manoeuvring tests:
❑ oscillatory tests in x- and y-direction and around ψ-axis;
❑ harmonic sway tests: pure sway;
❑ alternative sway tests: pure sway;
❑ harmonic yaw tests: pure yaw, yaw with drift with positive and negative forward speed;
❑ multi-modal tests.

Except for the bollard pull tests, Froude numbers are varied within the range [-0.032 ; 0.154], corresponding to full scale velocities of −3.4 to 16 knots. With a reference propeller rate n_0 (MCR) of 100 rpm full scale, propeller

revolutions have been varied from a minimum of 10% to 100% n_0 ahead and astern. In this way, a wide range of combinations of model speeds and propeller revolutions is covered so that the influence of low and ordinary ship velocities combined with varying telegraph positions can be examined.

4. EXPERIMENTAL RESULTS AND IMPLEMENTATION INTO THE SELECTED MATHEMATICAL MODEL.

4.1. Hull forces and moment

Results of captive model tests for hull forces and moment have been discussed in [4] although no special attention has been paid to low speed manoeuvring implications.

As the under keel clearance (UKC) diminishes from 20% of the ship's draught to 7%, a quadratic dependence of non-dimensional resistance force $X'^{(\beta)}$ on ship's speed V cannot be maintained (figure 1):

$$X''^{(\beta)} = \frac{X^{(\beta)}}{0.5\rho L_{PP}d\left(u^2 + v^2\right)} = \frac{X^{(\beta)}}{0.5\rho L_{PP}dV^2}$$

so that a higher order model must be introduced. Although some scatter is recognised at 20% UKC – probably due to measurement errors as longitudinal forces on a ship model of 4 m length are rather small – a mean value will be used in the mathematical model.

4.2. Propeller induced forces

Analysing the influence of drift on the thrust coefficient K_T during *stationary tests* a distinction is made between low speed manoeuvring ($F_n = 0.016$) and ordinary speed manoeuvring ($F_n \geq 0.049$). Tests at small drift angles ($|\beta| \leq 5$ deg) are also executed with varying rudder deflection.

In figure 2 an increasing drift angle leads to an increase of the measured thrust coefficient for all test runs (including tests with varying rudder angle). Stationary tests have been executed at propeller rates of 50% ($J' = 0.13$) and 100% ($J' = 0.06$) of the reference propeller rate n_0. An increasing drift angle gives a decreasing value for the apparent advance ratio J' as the longitudinal velocity component diminishes. At higher propeller rates the dependence of the thrust coefficient on the drift angle is almost symmetrical. At lower propeller rates a small asymmetry is observed.

Stationary tests with non-zero drift angle ($|\beta| \geq 10$ deg) and low model speed ($F_n=0.016$) give negative values for $1-w_P$ which means that the inflow velocity into the propeller disc is negative or open water results of quadrant 4 are used (increase of the thrust coefficient compared to quadrant 1). This tendency is similar to the development of increasing K_T values for bollard pull conditions as the propeller rate decreases (figure 3).

This relationship at low speed contrasts with the relationship shown in figure 4 for ordinary speed which is also recognised by other researchers. An increasing absolute value of the angle β leads now to a decreasing measured thrust coefficient K_T and consequently to a decreasing wake fraction w_P. At straight ahead motion the wake fraction is expected to be rather high.

4.3. Rudder induced forces

Modelling of rudder forces F_X and F_Y

The modelling technique of rudder forces described in equations (13) to (20) is generally accepted, but has the disadvantage that no distinction is made between the contribution of the ship's velocity on the one hand and the propeller induced slipstream velocity u_S on the other to the averaged velocity V_R at the rudder position. The same value of the averaged velocity at the rudder (18) can be obtained with a wide range of different combinations of $(1-w_R)u$ ($= u_{R0}$) and u_S (figure 5). In addition modifications to (18) are required to take account of the four quadrants of operation.

The ratio of the wake fraction at the rudder to the wake fraction at the propeller (ζ in equation (19)) is expected to be function of the apparent advance angle ε^* or the apparent advance coefficient J' (through the wake fraction w_P).

Multi-modal straight-line rudder tests (type A: constant propeller rate of turn and harmonically varying rudder angle) have been executed with a great variety of combined velocities and propeller rates for the four quadrants of operation. For the situations related to the first quadrant, two different ratios ζ_X and ζ_Y have been calculated corresponding respectively to the longitudinal and lateral rudder forces, F_X and F_Y. For three combinations of apparent advance coefficient J' (see table):

Combination	F_n	n (% n_0)
1 (J' = 0.255)	0.032	50
	0.065	100
2 (J' = 0.605)	0.077	50
	0.154	100
3 (J' = 1.512)	0.077	20
	0.154	40

ζ_Y is shown on figure 6 and identical values are expected for each combination. These combinations are selected in such a way that the propeller loading corresponds to an accelerating motion (combination 1), a motion near self propulsion (combination 2) and a decelerating motion (combination 3). Comparable values for each combination have been found for large rudder angles, while for moderate rudder angles (for example $|\delta_R| < 30$ deg for combination 3) equation (18) seems to have shortcomings especially in modelling manoeuvres different from self propulsion (propeller overload or low propeller revolutions).

In [5] the shortcoming of an averaged rudder velocity has been solved by introducing a *Rudder Loading* concept analogous to the propeller loading. The rudder loading depends on slipstream velocity u_S and speed of advance at the rudder u_{R0} so that a rudder loading angle is defined by (figure 6):

$$\xi = \text{Arctan}\left(\frac{u_{R0}}{u_S}\right) \qquad (21)$$

This concept has not been applied yet to the test results shown in figure 6 (results expected autumn 2005). The ratio of two in-line velocities in (21) to define a four quadrant angle is an artificial method in this case but provides relevant measures of the characteristic variations in flow geometry over the four quadrants.

Lateral rudder forces measured during captive multi-modal tests in quadrant 4 (stopping from sternway) are shown in figures 7 and 8. Due to the sternway of the ship model the rudder profile experiences two opposite flows. Propeller revolutions and consequently the propeller slipstream must be high enough to counteract the flow corresponding to the astern motion. At $F_n = -0.016$ the lateral rudder force F_Y at 50% of the reference propeller rate n_0 is less than 25% of the value measured at 100% n_0. For an increasing backward velocity ($F_n = -0.032$) the measured force F_Y is even negligible and a propeller telegraph position near HALF AHEAD is needed to induce some turning ability.

Modelling of interaction coefficients t_R, a_H and x'_H

The interaction coefficient a_H based on stationary oblique towing tests is shown on figures 9-11:

$$Y_R = (1 + a_H)F_Y$$

❏ For bollard pull tests ($F_n = 0$ or low speed manoeuvring) coefficient a_H is zero for all rudder deflections as no flow is created around the ship hull (figure 9).

❏ At increasing speed ($F_n = 0.116$) and straight ahead motion a_H increases as well (maximum of about 0.5) with a small influence of the rudder angle (figure 10, legend see figure 9).

❏ A drift angle of −5 deg gives an increase of a_H compared to the straight ahead motion depending on the rudder angle (values between 1 and 2.5, figure 11). The reduced lateral force referred to in figure 11 is the total force minus the lateral hull force due to drift.

❏ Based on figures 10 and 11, coefficient a_H depends on the apparent advance coefficient J' and the inflow angle into the rudder; following model is proposed [6]:

$$a_H = \frac{A_1 J'}{J'^3 + A_2} \qquad (22)$$

where coefficients A_1 and A_2 are defined as:

$$A_1 = 3a_{Hmax}J'^2_{max}$$
$$A_2 = J'^3_{max} \qquad (23)$$

making use of two parameters J'_{max} and a_{Hmax}, which means that coefficient a_H reaches a maximum value of a_{Hmax} at a propeller advance ratio J'_{max}. The apparent propeller advance ratio is based on the total ship velocity V during straight line and oblique towing tests:

$$J' = \frac{V}{nD_P} = \frac{\sqrt{u^2 + v^2}}{nD_P} \qquad (24)$$

For bollard pull tests (J'=0) and tests with very low propeller loading (J'→∞) hull coefficient a_H is expected to be zero.

Although the coefficient a_H is a function of the advance coefficient J' (combinations of velocity u and propeller rate n) the lateral force Y_R can only be modelled accurately if a distinction is made between low speed and ordinary speed (figure 12, constant drift angle of −5 deg). A

model based on all Froude numbers give an underestimation of the force Y_R at low speed.

The non-dimensional position x'_H of the rudder induced hull force $a_H F_Y$ is shown on figure 13 (for oblique towing tests). At ordinary speed ($F_n \geq 0.049$) this position is aft of midship and changes hardly except at small rudder angles ($|\delta_R| \leq 10$ deg). At low speed this position varies between 15% of the ship length aft of midship and midship position.

Comparable results for coefficient x'_H are obtained during PMM yaw tests with varying yaw rate angle γ (equation (5), figure 14). For a right-handed propeller a starboard rudder deflection (negative rudder angles) gives a more stable flow around the hull-propeller-rudder combination and additionally x'_H is more aft during a starboard turn compared to a port turn. Combining port rudder and rate of turn to starboard gives a negligible flow of the propeller into the rudder so that at high yaw rate angles the position x'_H is located far fore of midships.

5. OPPURTUNITIES AND LIMITATIONS

In chapter 4 some examples are given of the complexity of mathematical modelling for all combinations of ship velocity and propeller revolutions occurring during a harbour manoeuvre. Not all of the four quadrants are discussed at length and only a thorough validation of the existing mathematical model can give a full insight.

❑ Assessing the results of modelled coefficients such as wake fraction w_P and interaction coefficients due to rudder action based on captive model tests, special attention must be paid to the difference between low speed and ordinary speed manoeuvring.

❑ There is a necessity to adjust the existing models for the propeller and rudder induced forces to models, which incorporate the physical diversity of flow patterns in each of the four quadrants.

❑ This comprehensive test program is a valuable tool to evaluate the necessity of executing model tests in each quadrant of operation and can lead to the development of a standard program of captive model tests.

❑ Information about the field of application of a mathematical model must be available so that low speed manoeuvres will not be predicted based on manoeuvres typical for the design condition of a ship and if so, that the user of a simulator is aware of these facts and their consequences.

6. REFERENCES

[1] DAND I., Low speed manoeuvring criteria: some considerations. MARSIM 2003, Kanazawa, Japan.

[2] HWANG W.-Y. et all, An exploratory study to characterize ship maneuvering performance at slow speed. MARSIM 2003, Kanazawa, Japan.

[3] HARVALD SV.Aa. Wake and thrust deduction at extreme propeller loadings. Publications of the Swedish State Shipbuilding Experimental Tank, Nr. 61, Göteborg, 1967.

[4] ELOOT K., VANTORRE M. Development of a tabular manoeuvring model for hull forces applied to full and slender ships in shallow water. MARSIM 2003, Kanazawa, Japan.

[5] CHISLETT M.S. A generalized math model for manoeuvring. MARSIM'96, Copenhagen, Denmark, 1996.

[6] VANTORRE M., ELOOT K., HEYLBROECK B. Evaluation of mathematical models for propulsion and rudder forces by means of captive model tests with bulkcarriers in shallow water. Manoeuvrability'95, Ilawa, Polen, 1995.
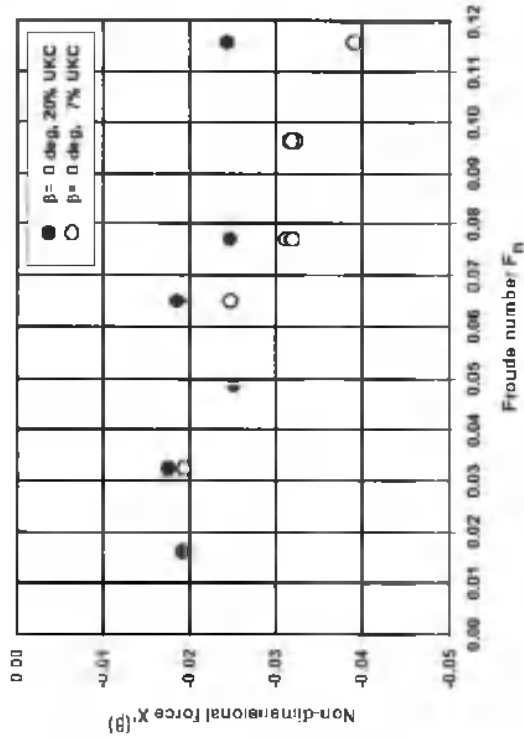
Figure 1 Non-dimensional force $X^{(\beta)}$ measured during stationary tests as function of Froude number
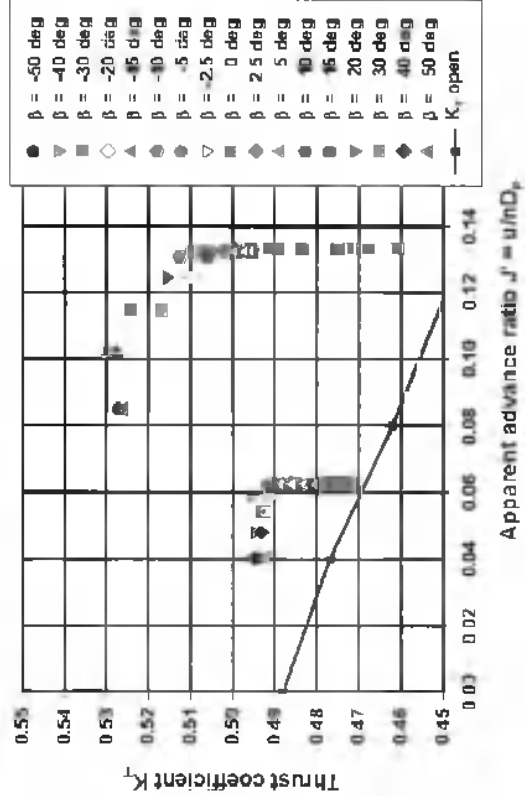

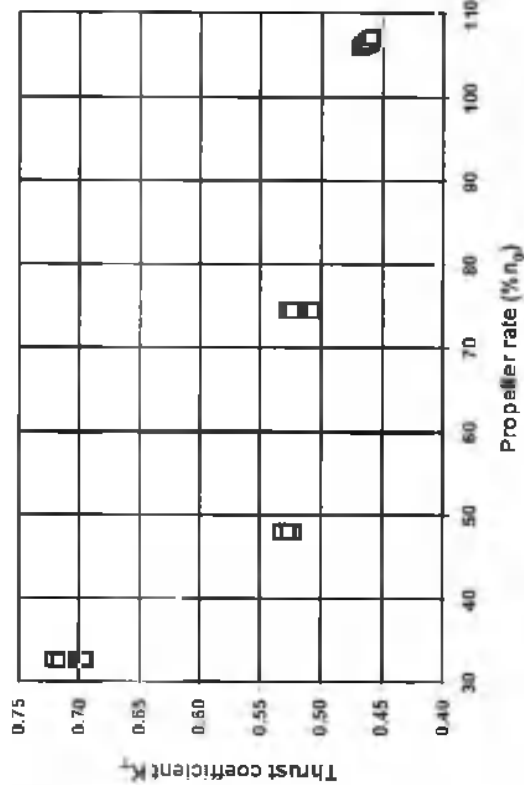**Figure 2** Influence of drift angle on propeller thrust coefficient K_T at low speed ($F_n=0.016$), quadrant 1

Figure 3 Propeller thrust coefficient K_T at bollard pull condition (rudder deflection), transition between quadrants 4 and 1
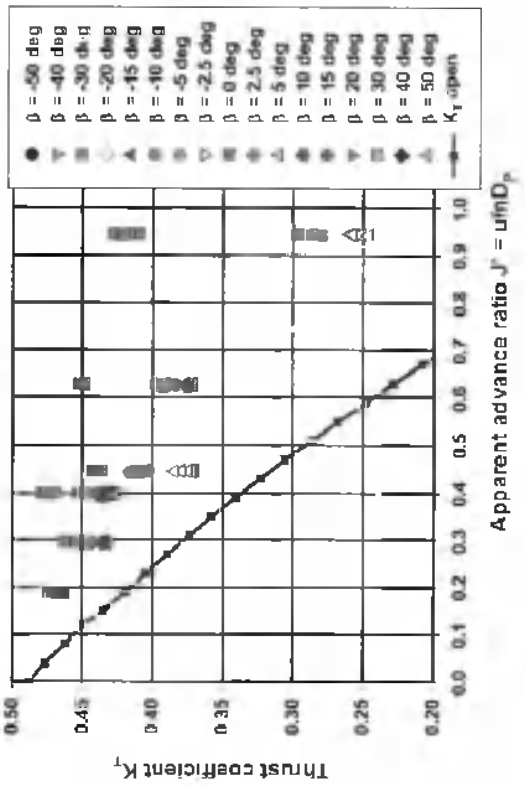

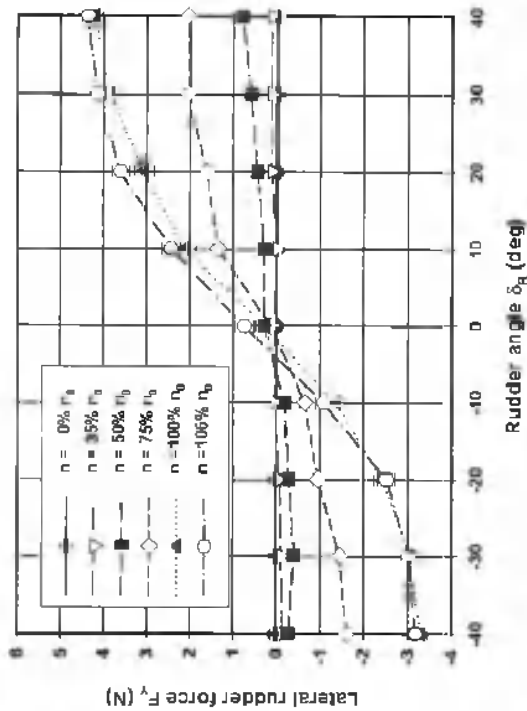**Figure 4** Influence of drift angle on propeller thrust coefficient K_T at ordinary speed ($F_n \geq 0.049$), quadrant 1

Figure 7 Tabular mode' of measured lateral rudder force, F_n=-0.016 (quadrant 4, stopping from sternway, multi-modal tests type A)
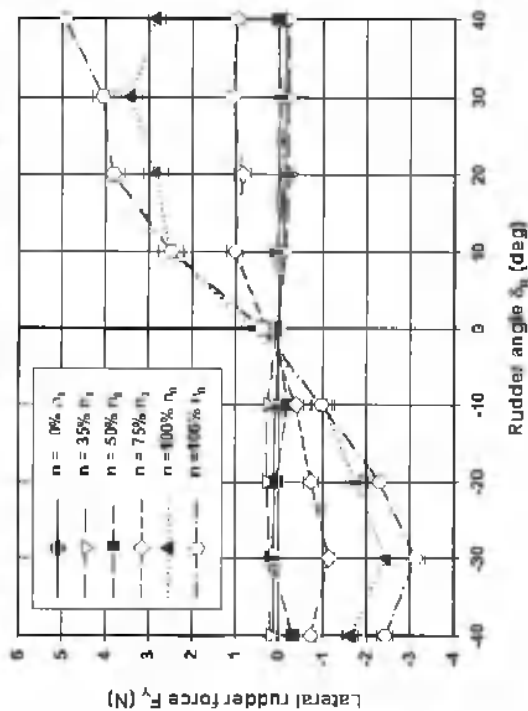
Legend (Figure 7):
- n = 0% n_b
- n = 35% n_b
- n = 50% n_b
- n = 75% n_b
- n =100% n_b
- n =106% n_b

Axes: Rudder angle δ_R (deg); Lateral rudder force F_Y (N)

Figure 8 Tabular mode' of measured lateral rudder force, F_n=-0.032 (quadrant 4, stopping from sternway, multi-modal tests type A)

Legend (Figure 8):
- n = 0% n_b
- n = 35% n_b
- n = 50% n_b
- n = 75% n_b
- n =100% n_b
- n =106% n_b

Axes: Rudder angle δ_R (deg); Lateral rudder force F_Y (N)

Figure 5 Rudder loading concept according to Chislett [CHI]

Labels: U_{R0}, U_S, U_{R0}, U_P

Figure 6 Ratio ζ_Y as function rudder angle δ_R for three combinations of apparent advance coefficient J', quadrant 1

Legend (Figure 6):
- F_n=0.032; n = 50% n_b
- F_n=0.065; n =100% n_b
- F_n=0.077; n = 50% n_b
- F_n=0.154; n =100% n_b
- F_n=0.077; n = 20% n_b
- F_n=0.154; n = 40% n_b

Axes: Rudder angle δ_R (deg); ζ_Y

Figure 11 Measured values and linear regression lines for coefficient $1+a_H$ based on stationary oblique towing tests ($\beta=-5$deg and $F_n=0.116$), quadrant 1

Figure 12 Tabular models for J'_{max} and a_{Hmax} based on oblique towing tests $\beta=-5$deg (low and ordinary speed manoeuvring, quadrant 1)
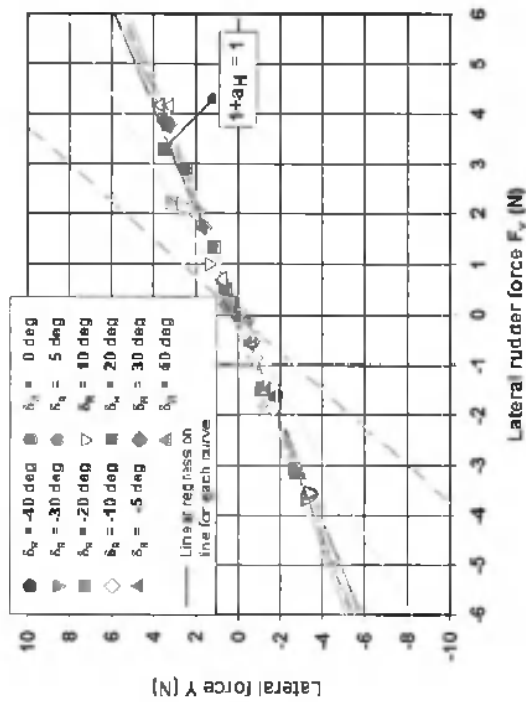

Figure 9 Measured values and linear regression lines for coefficient $1+a_H$ based on bollard pull tests ($F_n=0$), quadrant 1
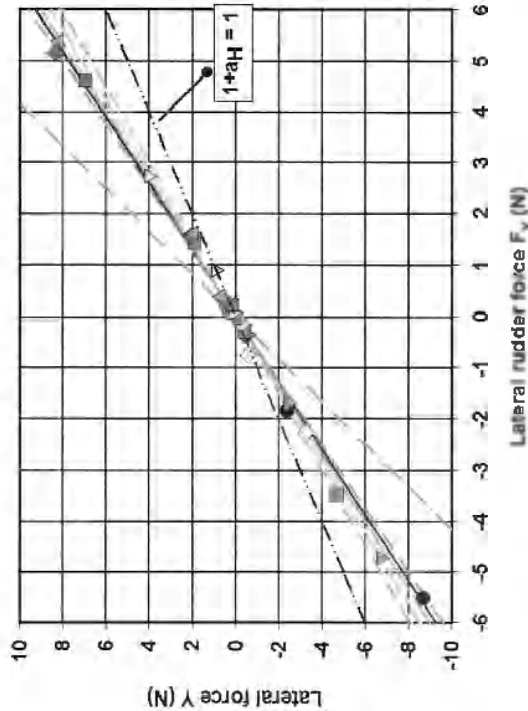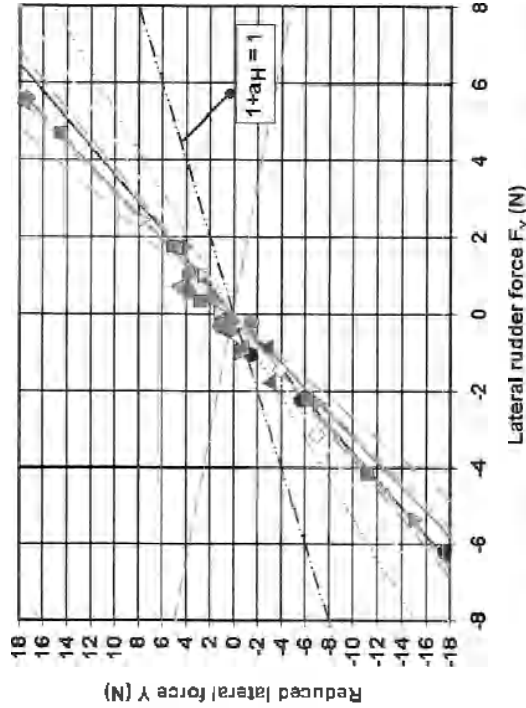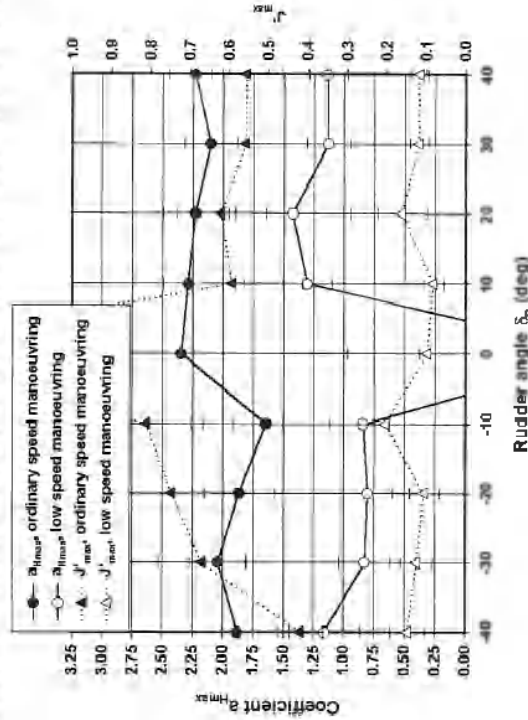

Figure 10 Measured values and linear regression lines for coefficient $1+a_H$ based on stationary straight line tests ($F_n=0.116$), quadrant 1
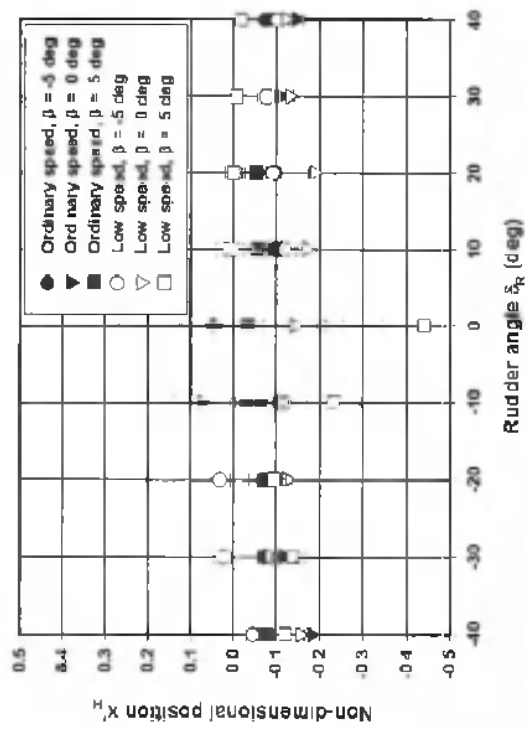
Figure 13 Non-dimensional position x'_H based on stationary straight line and oblique towing tests, quadrant 1
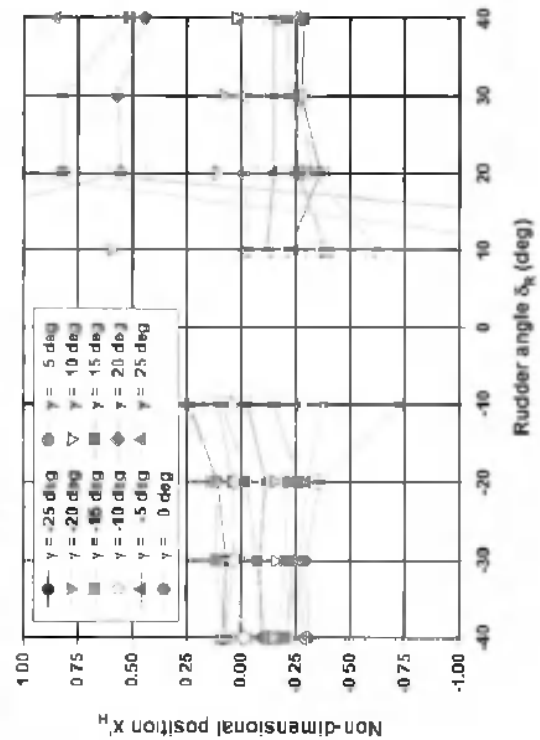

Figure 14 Non-dimensional position x'_H for PMM yaw tests with F_n=0.065, n=75% n_0, quadrant 1